Journal of Hydrology 670 (2026) 135210

Contents lists available at ScienceDirect

Journal of Hydrology

journal homepage: www.elsevier.com/locate/jhydrol

Research papers

Flow resistance continuity from overland to rill flows: evidence from experimental data and theoretical implications

Vincenzo Palmeri [a,b], Alessio Nicosia [a,*], Costanza Di Stefano [a], Vito Ferro [a,b]

[a] Department of Agricultural, Food and Forest Sciences, University of Palermo, Viale delle Scienze, Building 4, 90128 Palermo, Italy
[b] NBFC, National Biodiversity Future Center, 90133 Palermo, Italy

A R T I C L E I N F O

This manuscript was handled by Ashok Mishra, with the assistance of Emad Hasan, Associate Editor

Keywords:
Soil erosion
Rill
Overland flow
Flow resistance

A B S T R A C T

Knowledge of the friction factor of overland and channelized rill flows moving over rough hillslopes is required for modeling soil erosion and transport processes. The available literature flume investigations are characterized by different values of the ratio between the hydraulic radius R and the water depth h, and distinguish the two hydraulic cases corresponding to overland (R quasi equal to h) and rill flows ($R/h < 1$). In this paper, literature flume measurements performed in smooth and rough channels, which are characterized by a fixed bed and a grain resistance condition, were firstly used to highlight the experimental evidence that a continuity in flow resistance from overland (hydraulic radius R quasi equal to water depth h) to rill flows ($R/h < 1$) can be stated. This analysis pointed out that the measured highest f values correspond to very wide rectangular cross-sections (VWR) and narrow rectangular cross-sections (NR), while for the intermediate geometric conditions, the lowest friction factor values were measured. This detected transition from VWR to NR cross-sections implies a transition in flow resistance that can be represented in the flow resistance equation by R/h. In particular, the proposed flow resistance law was theoretically deduced considering rectangular cross-sections characterized by different R/h values and calibrated by the available datasets. The agreement between the measured f values and those calculated by the theoretical flow resistance equation was characterized by errors, which were normally distributed, less than or equal to $\pm$ 10% for 96.8% of the cases and less than or equal to $\pm$ 5% for 82.0% of the cases. The proposed flow resistance equation is applicable for channels with a rectangular cross-section varying from VWR (overland flows) to NR (rill flows).

1. Introduction

The soil erosion process has received much scientific attention as it is considered to be one of the most critical forms of degradation, has been accelerated by human activity, and is related to land use changes (Borrelli et al., 2017). The study of interrill (with overland flows) and channelized (rill and gully) erosion is relevant as these erosion components are responsible for the majority of soil loss from hillslopes (Di Stefano et al., 2022a; Pampalone et al., 2023).

The simplest process-oriented soil erosion model (Nearing et al., 1989; Flanagan and Nearing, 1995; Ferro, 2010) is divided into two components: one representing the interrill erosion processes (Mutchler and Young, 1975; Abrahams et al., 1994; Toy et al., 2002; Nicosia et al., 2024a) and the other representing rill erosion (Casalì et al., 2006; Capra et al., 2009; Di Stefano and Ferro, 2011; Carollo et al., 2015; Bagarello et al., 2018). The main justification for using this two-component-schematization is that the physical variables controlling interrill and rill erosion are different (Flanagan et al., 2007). As an example, hillslope length has no effect on interrill erosion, whereas rill erosion increases with slope length (Toy et al., 2002). However, process-oriented models require the estimate of the mean flow velocity, which is related to sediment transport capacity and affects erosion and deposition phenomena.

Overland flow is studied as a shallow open-channel flow moving along a slope under the effect of gravity. The analysis of overland flow is not simple, as the hydraulic variables are difficult to define using basic hydraulic techniques that are only marginally applicable (Emmett, 1970; Nicosia et al., 2021a). Overland flows are characterized by subcritical to supercritical flow depths, and roll waves may occur as a result of the flow's instability (Emmett, 1970; Govers et al., 2000; Fang et al., 2021; Wang et al., 2014, 2021), especially for increasing slope (Zanuttigh and Lamberti, 2002) or flow rate. For the overland flow

* Corresponding author.
E-mail address: alessio.nicosia@unipa.it (A. Nicosia).

https://doi.org/10.1016/j.jhydrol.2026.135210
Received 8 September 2025; Received in revised form 10 December 2025; Accepted 23 February 2026
Available online 27 February 2026

condition, for which the flow width is usually much greater than the flow depth, the hydraulic cross-section can be assumed to be a very wide rectangular one. Furthermore, the water surface tends to be parallel to the hillslope (considered as a uniform slope) asymptotically, and the flow can be considered uniform (Nicosia et al., 2024b).

Rills are small channels characterized by steep slopes and water depths varying from some millimeters to several centimeters (Fig. 1). Modelling of interrill and rill erosion processes requires the knowledge of hydraulic variables such as surface width, water depth, mean flow velocity, and roughness coefficient, which must be defined in addition to flow discharge (Foster et al., 1984; Gilley et al., 1990; Govers, 1992; Nearing et al., 1997; Peng et al., 2015; Ferro, 2018a).

The open channel flows moving as overland or in a rill are generally affected by grain resistance (due to roughness height), bed forms, and sediment transport. Notwithstanding hillslope overland flow, channelized rill flows, and river flows present both similarity and difference due to the geometrical scale and the effect of the involved hydraulic processes, most of the physically-based erosion models (De Roo et al., 1994; Laflen et al., 1991; Morgan et al., 1998; Nouwakpo et al., 2016) use the well-known Chezy's equation (Ferro, 1999; Smith et al., 2007; Powell, 2014):

$$V = C\sqrt{Rs} = \frac{s^{1/2}R^{2/3}}{n} = \sqrt{\frac{8gRs}{f}} \tag{1}$$

in which V is the mean flow velocity (m s^{-1}), C is the Chezy coefficient ($m^{1/2}$ s^{-1}), n is the Manning coefficient ($m^{-1/3}$ s), f is the dimensionless Darcy–Weisbach friction factor, R (m) is the hydraulic radius, s (−) is the slope steepness, and g (m s^{-2}) is the acceleration due to gravity. Many erosion models use Manning's equation to model overland flow (Hessel et al., 2003; Shen et al., 2023a), while the Darcy–Weisbach friction factor is used in WEPP (Water Erosion Prediction Project) (Foster et al., 1995; Govers et al., 2007; Ferro and Nicosia, 2020). Furthermore, field studies commonly use the Darcy–Weisbach friction factor to model flow resistance (Smith et al., 2007; Nicosia et al., 2020a). Equation (1) is commonly applied for overland flows, substituting the hydraulic radius R with the water depth h (m), as the flow width is usually much greater than the flow depth.

While for rills the flow regime is generally turbulent, for overland flows, the Reynolds number Re generally assumes values corresponding to the laminar or transition regime; however, the flow cannot be considered laminar when disturbances due to impacting rainfall and hillslope surface irregularities occur. For this reason, Horton (1945) postulated that an overland flow over a natural hillslope is a "mixed flow"; in other words, it is characterized by areas with fully turbulent flow mixed with areas where the flow is laminar. The variability of Re from overland to rill flows should be considered when a single flow resistance equation is used to express both these hydraulic conditions.

A challenge for uniform open-channel flow hydraulics is the theoretical deduction of the flow-resistance law by integration of a known flow-velocity distribution in the cross-section (Ferro, 1997, 2003, 2017; Powell, 2014). Dimensional analysis can be usefully applied to solve this problem (Barenblatt, 1987), as the flow-resistance law and the flow-velocity distribution can be expressed by functional relationships representing the examined physical process.

Ferro (2017) deduced a new resistance equation for open-channel flows applying dimensional analysis and self-similarity theory (Barenblatt, 1991, 1993). This theory was used, as it will be shown in the next paragraph, to establish the power velocity distribution whose integration allows for obtaining a theoretical expression of the Darcy–Weisbach friction factor.

It is noteworthy that this theoretical flow resistance equation has successfully applied for overland (Nicosia et al., 2020a, 2020b, 2024b, 2025a, 2025b) and rill flows (Di Stefano et al., 2018, 2019, 2021a, 2022b, 2024a; Carollo et al., 2021; Nicosia et al., 2019; Palmeri et al., 2018).

Flume measurements allow the experimental study of the uniform flow motion in a straight rill channel with a mobile or fixed bed, while field experiments allow for investigating a complex rill geometry (Fig. 1). For a given soil roughness, Di Stefano et al. (2024a) compared measurements performed in fixed-bed rill channels incised in plots with data obtained in rectangular rill flumes. This analysis, developed for two

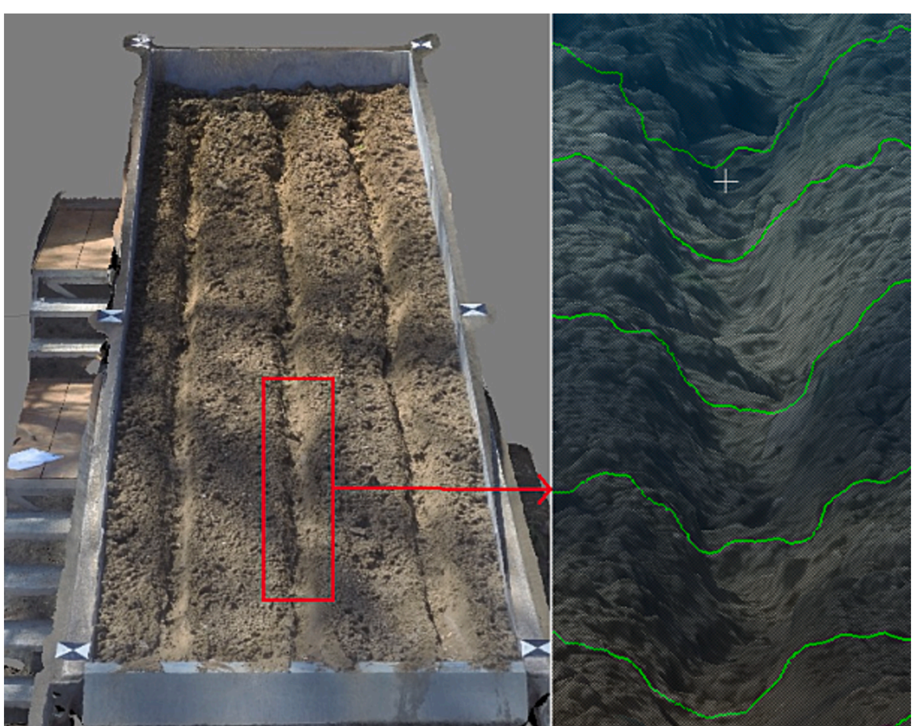

Fig. 1. Example of a complex rill geometry.

different soils, stated that the influence of different soil roughness on f is limited in comparison with that due to rill cross-section shape.

Recently, Lucchese et al. (2025) carried out some experimental runs in rectangular rill channels using a smooth flume and three fixed-bed flumes whose bottom and walls were covered by soils with different textures (clay-loam, sandy-loam and clay). In agreement with the results by Di Stefano et al. (2024a), this investigation demonstrated that the influence of different soil roughness (grain resistance) on f is very limited.

Even if flow resistance has been widely studied for overland and rill flows investigating the influence of different variables on flow resistance, the behavior of flow resistance in the transition from overland to rill flows remains unexplored.

In this paper, the flume measurements by Savat (1980) and Lucchese et al. (2025) carried out for smooth and rough channels, which are characterized by a rectangular cross-section, a fixed bed and a grain resistance condition, were used. Additional effects, such as rainfall impact (Nicosia et al., 2025a; 2025b; Shen et al., 2021; 2023b), vegetation and biological soil crust (Dan et al., 2023; 2024; Di Stefano et al., 2024b), and flow sediment transport (Liu et al., 2023; Nicosia et al., 2021b), were not considered as the main aim of this investigation is to study the width cross-section effects, from very wide rectangular (VWR) to narrow rectangular (NR), on flow resistance due only to grain roughness.

Measurements performed for different values of the ratio between the channel width L and the water depth h and, as a consequence, different values of the ratio between the hydraulic radius R and h, were employed to demonstrate the experimental evidence that continuity in flow resistance from overland (R quasi equal to h) to rill flows ($R/h < 1$) (Smith et al., 2007; Nicosia et al., 2024a) can be established. Finally, using these flume measurements available in the literature, a theoretical flow resistance equation was calibrated using a continuity approach from overland to rill flows.

2. Materials and methods

2.1. Available experimental data

The first data set consists of the measurements by Savat (1980), which were carried out using seven sloping flumes (s varying from 0.8% to 58%), 3 m long and 0.117 m wide. One flume was smooth (plastic) and six others are covered by sediments fixed on the channel bed (Loess, Tongeriaan sand, Brusseliaan sand, Loess with gravel, Tongeriaan sand with gravel, Brusseliaan sand with gravel). Therefore, the flow resistance contribution due to smooth walls for these runs is negligible. In the paper by Savat (1980), the measurements (702 experimental runs) are plotted in graphs representing the experimental pairs Re-f, in which the Reynolds number Re is calculated as $4V\,h/\nu_k$ and ν_k is the kinematic viscosity, for different slope steepness conditions. For each investigated condition, using the plotted pairs (Re, f), the mean velocity V and the water depth h values were calculated by the following relationships:

$$V = \sqrt[3]{\frac{2gs\nu_k}{\left(\frac{f}{Re}\right)}} \tag{2}$$

$$h = \frac{Re\nu_k}{V} \tag{3}$$

The second dataset is constituted of the experimental runs by Lucchese et al. (2025), which also include the measurements by Di Stefano et al. (2021b), Nicosia et al. (2021a), and Di Stefano et al. (2024a). These 196 runs were performed in a sloping flume (s varying from 0.1% to 15%), 5 m long, 0.04 m deep, and 0.078 m wide (Fig. 2). A small pipe supplied the discharge entering the flume, and the water coming out was collected in a tank. The experimental runs were performed using a smooth flume (aluminium) and three flumes having bed and walls characterized by different roughness conditions, which were obtained by fixing a sieved soil. In these cases, especially for high values of water depth, the total flow resistance is affected by the additional flow resistance due to wall roughness. In detail, one flume was covered by a clay-loam soil (36.4% sand, 30.9% silt, and 32.7% clay), while the others were covered by a sandy-loam (55.8% sand, 31.4% silt, and 12.8% clay) and a clay soil (5% sand, 33% silt, and 62% clay). Each experimental run was characterized by given values of slope s, discharge Q, and water depth h. The flow discharge was measured by the volumetric technique (i.e., measuring the filling time of a bucket having known volume), while the water depth h was measured by a point gauge (accuracy 0.1 mm) placed in the flume axis, 2 m apart from the inlet. For each run, the hydraulic cross-section area was calculated by multiplying the flow width L by h, and the mean flow velocity V was calculated as the ratio between the measured Q and cross-section area.

Fig. 2. View of the flume used for the experiments by Lucchese et al. (2025).

For both the databases, the Reynolds number $Re = V\,h/\nu_k$, in which ν_k is the kinematic viscosity, and the Froude number $F = V/(g\,h)^{0.5}$ were also calculated.

For each dataset, Table 1 lists the range of the investigated slope s, discharge Q (L/s), ratio h/L, ratio R/h, Reynolds number Re, and Froude number F. The values of L/h and R/h listed in Table 1 demonstrate that the dataset by Savat (1980) is dominated by very wide rectangular cross-

Table 1
Characteristic data of the ~~two~~ used datasets.

Variable	Savat (1980)	Lucchese et al. (2025)	This investigation
s (−)	0.008 – 0.58	0.001 – 0.15	0.0251 – 0.32
Q (L s^{-1})	0.005 – 0.84	0.19 – 0.88	0.20 – 0.88
L/h	9.7 – 270.3	2.6 – 21.7	4.4 – 19.2
R/h	0.83 – 0.99	0.57 – 0.91	0.69 – 0.91
$Re = V\,h/\nu_k$	33—5623	1911—10247	2028—8427
F	0.22 – 11.7	0.46 – 7.67	1.4 – 4.5

sections (R/h near to 1 and $L \gg h$), which are characteristic of overland flow conditions, while data by Lucchese et al. (2025), which are typical of rill flows, are characterized by rectangular cross-section (R/h varying from 0.57 to 0.91 and a more narrow range of L/h).

Considering that the dataset by Savat (1980) is dominated by overland flow conditions ($0.83 \leq R/h \leq 0.99$), while the dataset by Lucchese et al. (2025) is typical of rill flows ($0.57 \leq R/h \leq 0.92$), it is worth noting that the pairs (h, R/h) plotted in Fig. 3a allow for distinguishing three different ranges. The first range ($h \leq 0.36$ cm, $0.92 \leq R/h < 0.99$) corresponds to overland flows only investigated by Savat (1980), the second range is a transition zone from overland to rill flows ($0.36 < h \leq 1.21$ cm, $0.76 \leq R/h < 0.92$) and the third range ($h > 1.21$ cm, $0.76 < R/h < 0.57$) corresponds to rill flows only investigated by Lucchese et al. (2025).

Fig. 3b shows the frequency distributions of the ratio R/h corresponding to the dataset by Savat (1980) ($0.83 \leq R/h \leq 0.99$), the smooth configuration by Lucchese et al. (2025) ($0.73 \leq R/h \leq 0.91$), and the rough configurations by Lucchese et al. (2025) ($0.57 \leq R/h \leq 0.86$).

Fig. 3c shows the frequency distributions of the Darcy–Weisbach friction factor values corresponding to the dataset by Savat (1980) (overland flows), the smooth configuration by Lucchese et al. (2025) (transition), and the rough configurations by Lucchese et al. (2025) (prevalently rill flows).

A total of 898 data were available, and the pairs (Re, F), plotted in Fig. 4, show that the flows investigated by Savat (1980) are prevalently laminar, while those by Lucchese et al. (2025) are mainly turbulent flow conditions (Table 1).

2.2. Measurements carried out in this investigation

The experimental investigation was carried out using the same small flume used by Lucchese et al. (2025) (Fig. 2), which is 5 m long, 0.08 m wide, and 0.04 m high, placed at the experimental area of the Department of Agriculture, Food, and Forest Sciences of the University of Palermo. The bed and the walls of the flume were covered with natural zeolite particles with a mean roughness height of 0.505 mm. These 85 runs were performed using sixteen slopes (s = 2.5, 4.4, 6.1, 8.7, 9, 11, 13, 15, 16, 18, 22, 24, 26, 28, 30, and 32%) and five discharges (Q = 0.20 to 0.85 L s^{-1}) per slope were investigated. The volumetric method was used to measure the discharge, and a point gauge with an accuracy of ± 0.1 mm was used to measure the flow depth, h. The gauge was placed in the flume axis, two meters from the inlet section.

In this case, the R/h values range from 0.69 to 0.9 (Fig. 3b). For this dataset, Table 1 also lists the range of the investigated slope s, discharge Q (L/s), ratio h/L, ratio R/h, Reynolds number Re, and Froude number F. The pairs (Re, F), plotted in Fig. 4, show that the flows of this investigation are supercritical and turbulent (Table 1).

Fig. 3c shows the frequency distribution of the Darcy–Weisbach friction factor values corresponding to the dataset obtained in this study, which overlaps with the rough configurations by Lucchese et al. (2025) (prevalently rill flows).

2.3. The theoretical flow resistance equation

The use of dimensional analysis and self-similarity theory (Barenblatt, 1987) allows for theoretically deducing the flow velocity distribution in an open-channel flow (Ferro, 2017, 2018a, 2018b) having a rectangular cross-section with a width L. The ratio h/L allows for representing rectangular cross-sections with a geometry variable from very wide rectangular (VWR) ($L \gg h$, $h/L \rightarrow 0$ and $R/h \rightarrow 1$), representing an overland flow condition, to a narrow rectangular (NR) ($h \gg L$, $h/L \rightarrow \infty$, and $R/h \rightarrow 0$), representing a rill channel flow. For representing these geometrical conditions, the local flow velocity distribution $v(y)$ along a given vertical can be expressed by the following functional equation (Barenblatt, 1987; 1993; Ferro, 1997):

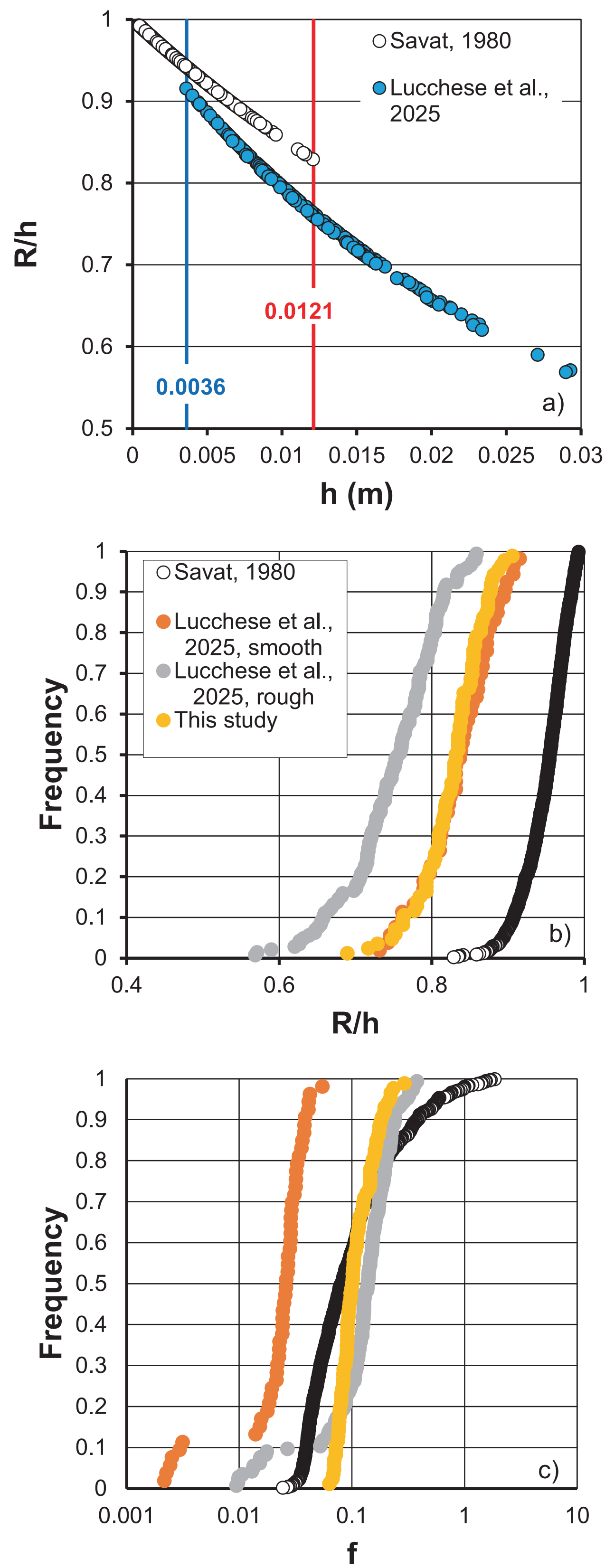

Fig. 3. Relationship between the values of flow depth h and ratio R/h for the investigated datasets (a), frequency distributions of R/h values corresponding to the different datasets (b), and frequency distributions of f values corresponding to the different datasets (c).

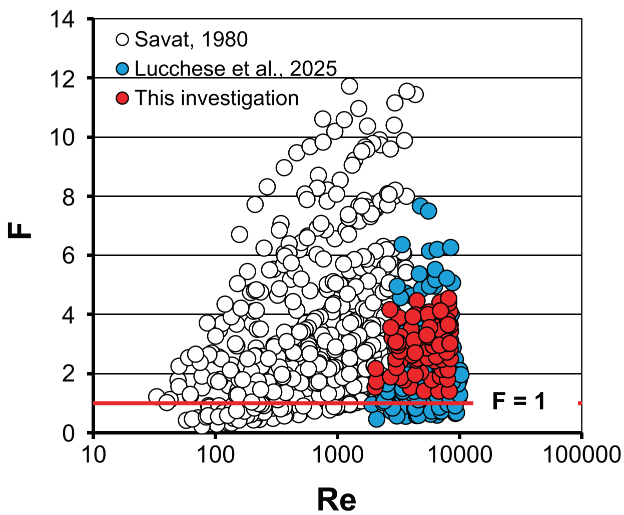

Fig. 4. Pairs (Re, F) for the investigated datasets.

$$\phi\left(\frac{dv}{dy}, y, L, h, d, u_*, s, \rho, \mu, g\right) = 0 \tag{4}$$

in which ϕ is a functional symbol, y is the distance from the bottom, d is a characteristic diameter of the soil particles, $u_* = \sqrt{gRs}$ is the shear velocity, ρ is the water density, and μ is the water viscosity.

Applying the Π-theorem (Barenblatt, 1987), Equation (4) can be rewritten in the following dimensionless form:

$$\Pi_1 = \phi_2(\Pi_2, \Pi_3, \Pi_4, \Pi_5, \Pi_6, \Pi_7) \tag{5}$$

in which Π_1, Π_2, Π_3, Π_4, Π_5, Π_6, and Π_7 are dimensionless groups and ϕ_2 is a functional symbol.

Using as dimensional independent variables y, u_*, and μ to deduce the dimensionless groups, Equation (5) can be rewritten as follows (Ferro, 2018b; Nicosia et al., 2020a):

$$\frac{y}{u_*}\frac{dv}{dy} = \phi_2\left(\frac{L}{y}, \frac{h}{y}, \frac{d}{y}, s, \frac{u_* y}{\nu_k}, \frac{gy}{u_*^2}\right) \tag{6}$$

As Barenblatt (1987) suggested that "*In some cases, it turns out to be convenient to choose new similarity parameters – products of powers of the similarity parameters obtained in the previous step*", the following dimensionless groups are deduced:

$$\Pi_{2,3} = \frac{1}{1 + 2\frac{\Pi_3}{\Pi_2}} = \frac{1}{1 + 2\frac{h}{y}\frac{y}{L}} = \frac{1}{1 + 2\frac{h}{L}} = \frac{R}{h} \tag{7}$$

$$\Pi_{3,6} = \sqrt{\frac{8}{f}}\Pi_3\Pi_6 = \frac{V}{u_*}\frac{h}{y}\frac{u_* y}{\nu_k} = \frac{Vh}{\nu_k} = Re \tag{8}$$

$$\Pi_{4,3} = \frac{\Pi_3}{\Pi_4} = \frac{h}{y}\frac{y}{d} = \frac{h}{d} \tag{9}$$

$$\Pi_5 = s \tag{10}$$

$$\Pi_6 = \frac{u_* y}{\nu_k} \tag{11}$$

$$\Pi_{7,3} = \sqrt{\frac{8}{f}}\frac{1}{\Pi_7^{1/2}\Pi_3^{1/2}} = \sqrt{\frac{8}{f}}\frac{u_*}{g^{1/2}y^{1/2}}\frac{y^{1/2}}{h^{1/2}} = \frac{\sqrt{\frac{8u_*^2}{f}}}{g^{1/2}h^{1/2}} = \frac{V}{\sqrt{gh}} = F \tag{12}$$

Since Ferro (2018b) demonstrated that F takes also into account the depth sediment ratio h/d, the functional relationship (6) can be rewritten as follows:

$$\frac{y}{u_*}\frac{dv}{dy} = \phi_3\left(\frac{R}{h}, Re, s, F, \frac{u_* y}{\nu_k}\right) \tag{13}$$

where ϕ_3 is a functional symbol.

Assuming the Incomplete Self-Similarity (ISS) hypothesis in $u_* y/\nu_k$ (Barenblatt and Monin, 1979; Barenblatt and Prostokishin, 1993; Ferro, 2017), Equation (13) can be integrated (Barenblatt and Prostokishin, 1993; Ferro and Pecoraro, 2000), and the following power velocity profile is obtained:

$$\frac{v}{u_*} = \Gamma\left(\frac{R}{h}, Re, s, F\right)\left(\frac{u_* y}{\upsilon_k}\right)^{\delta} \tag{14}$$

in which Γ is a function of the dimensionless groups R/h, Re, s, and F, to be defined by velocity measurements, and δ is an exponent calculated by the following theoretical equation (Barenblatt, 1991; Castaing et al., 1990)

$$\delta = \frac{1.5}{\ln Re} \tag{15}$$

Setting $y = \alpha\, h$ as the distance from the bottom at which the local velocity is equal to the cross-section average velocity V, Equation (12) allows for obtaining the following value of the Γ function (Ferro, 2017; Ferro and Porto, 2018):

$$\Gamma = \frac{V}{u_*\left(\frac{u_* \alpha h}{\nu_k}\right)^{\delta}} \tag{16}$$

in which α is a coefficient, smaller than unit, which takes into account that the average velocity V is located under the water surface and that the mean velocity profile, whose integration gives V, is calculated by averaging, for each distance y, the velocity values v measured in different verticals.

Ferro (2017) proposed the following theoretical equation for calculating α:

$$\alpha = \left[\frac{2^{1-\delta}}{(\delta+1)(\delta+2)}\right]^{1/\delta} \tag{17}$$

Applying the ISS for all the dimensionless groups included in the Γ functional relationship (see Equation (14), the following estimate Γ_v is obtained:

$$\Gamma_v = a\frac{F^b}{s^c Re^e (R/h)^i} \tag{18}$$

in which the coefficients a, b, c, e, and i have to be experimentally determined. For an overland flow, assuming $R = h$, Eq. (18) is equal to the relationship proposed by Nicosia et al. (2022).

The Darcy–Weisbach friction factor f is obtained by integrating the power velocity distribution (Equation (14) (Ferro, 2017; Ferro and Porto, 2018; Nicosia et al., 2022):

$$f = 8\left[\frac{(\delta+1)(\delta+2)}{2^{1-\delta}\Gamma 4.4817}\right]^{\frac{2}{1+\delta}} \tag{19}$$

The application of Equation (19) requires the calculation of δ by Equation (15) and the estimate of $\Gamma = \Gamma_v$ by the calibrated Equation (18).

Combining Eq. (19) and (18), the following flow resistance equation is obtained:

$$f = 8\left[\frac{(\delta+1)(\delta+2)}{2^{1-\delta}a 4.4817}\right]^{\frac{2}{1+\delta}}\left(\frac{s^c Re^e (R/h)^i}{F^b}\right)^{\frac{2}{1+\delta}} \tag{20}$$

2.4. Statistical analysis

The agreement between the measured Darcy–Weisbach friction factor and those calculated by the theoretical flow resistance equation was evaluated by the root mean square error, *RMSE*, which is defined as:

$$RMSE = \sqrt{\frac{\sum_{i=1}^{N}\left(y_{m,i} - y_{c,i}\right)}{N}} \tag{21}$$

in which N is the sample size, and $y_{m,i}$ and $y_{c,i}$ are the measured and the calculated values of the examined dependent variable (Γ or *f*), respectively.

The agreement between measured and calculated *f* values was also controlled by the empirical frequency distribution of the errors in estimate $E = 100\ (f_c - f_m)/\ f_m$, in which f_c and f_m are the calculated and measured values of the Darcy–Weisbach friction factor, respectively.

Moreover, the *f* data for given range of R/h were subjected to One-Way ANOVA using "SPC for Excel" add-in software for Excel (BPI Consulting, LLC), assuming 95% as the confidence interval. Thus, statistical significance was attributed to p-value < 0.05.

The percent bias, P_{BIAS}, was also calculated according to Gupta et al. (1999):

$$P_{BIAS} = 100\frac{\sum_i^N (f_m - f_c)}{\sum_i^N f_m} \tag{22}$$

This statistic measures the average tendency of the calculated values f_c to be higher or lower than their measured counterparts f_m. The optimal value of this statistic is zero. Positive values indicate a model bias toward underestimation, whereas negative values indicate a bias toward overestimation.

3. Results

3.1. Evidence from experimental data

The available 898 data were first ordered with reference to specific R/h ranges, and the number N of data for each range is listed in Table 2. At first, these ranges were chosen considering that most of the experimental data by Savat (1980) correspond to overland flow conditions ($0.99 \le R/h \le 0.94$), while the majority of measurements by Lucchese et al. (2025) refer to rill flow conditions ($0.89 < R/h \le 0.57$) and that the remaining investigated R/h values can be attributed to a transition from VWR to NR (Fig. 3b). For each investigated R/h range, the mean value of the friction factor μ (*f*) and the standard deviation σ(*f*) are listed in Table 2.

For each investigated R/h range, the empirical frequency distribution of the Darcy-Weisbach friction factor is plotted in Fig. 5. This figure demonstrates that the highest *f* values correspond to the rectangular very wide cross-sections ($0.99 \le R/h \le 0.94$), typical of overland flows,

Table 2
Subdivision of the experimental data in R/h ranges and reference data base.

R/h range	N	Dataset	Cross-section type	μ (*f*)	σ(*f*)
$0.99 \le R/h \le 0.94$	474	Savat (1980)	VWR	0.213	0.280
$0.94 < R/h \le 0.90$	182	179, Savat (1980) 3, Lucchese et al. (2025)	Transition	0.074	0.047
$0.90 < R/h \le 0.80$	117	49, Savat (1980) 68, Lucchese et al. (2025)	Transition	0.086	0.085
$0.80 < R/h \le 0.57$	125	Lucchese et al. (2025)	NR	0.117	0.073

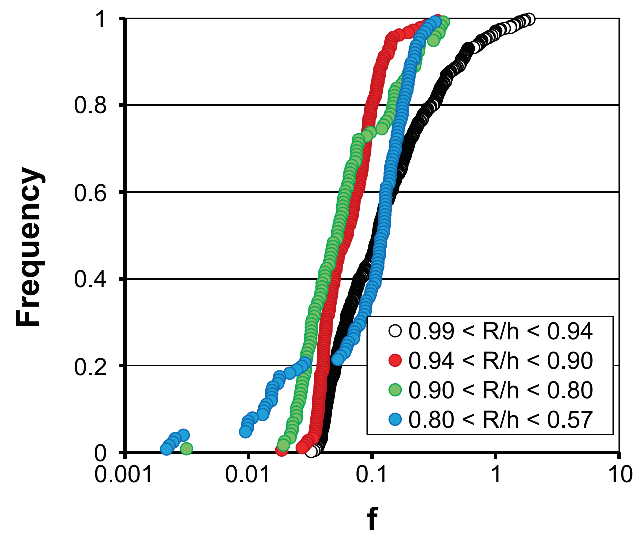

Fig. 5. Empirical frequency distribution of the Darcy–Weisbach friction factor corresponding to four investigated R/h ranges.

and to the rectangular narrow sections ($0.80 < R/h \le 0.57$), corresponding to rill conditions. This result is also confirmed by the mean values μ (*f*) listed in Table 2. Fig. 5 also shows that the distributions corresponding to the R/h ranges of 0.94–0.90 and 0.90–0.80, which represent the flow resistance transition from VWR to NR cross-sections, are almost overlaid and are characterized by *f* values generally less than those of the extreme conditions (VWR, NR). The ANOVA test was also performed to verify if the empirical cumulative frequency distribution of *f* corresponding to a given R/h range (for example, $0.99 \le R/h \le 0.94$ in Fig. 5) is statistically different from the other distributions concerning the different R/h ranges (for example, $0.94 < R/h \le 0.90$, and $0.90 < R/h \le 0.80$ in Fig. 5). This analysis demonstrated that the hypothesis that the statistical distributions shown in Fig. 5 have to be considered statistically coincident cannot be accepted.

A further analysis of the empirical cumulative frequency distributions corresponding to selected ranges of R/h characterized by the same number of data (sample size of 150) was also developed (Fig. 6). This analysis demonstrated that the highest *f* values correspond to overland flows (ranges $0.99 \le R/h \le 0.97$, $0.97 < R/h \le 0.96$, and $0.96 < R/h \le$

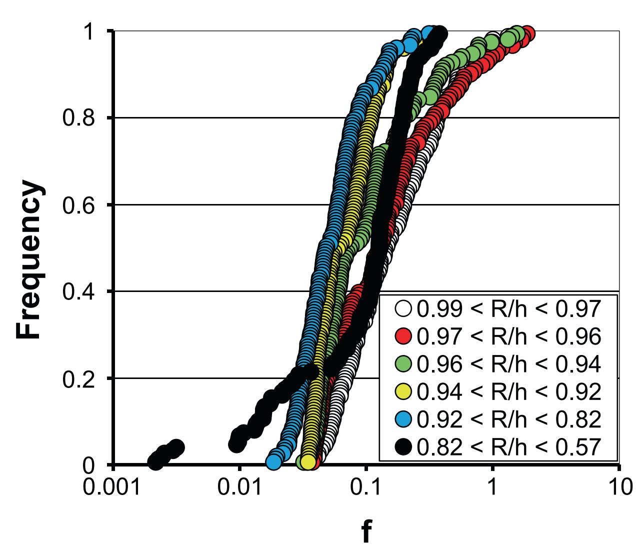

Fig. 6. Empirical frequency distribution of the Darcy–Weisbach friction factor corresponding to six investigated R/h ranges.

0.94) and rill flows ($0.82 < R/h \leq 0.57$). Moreover, when the R/h ranges decrease from $0.99 \leq R/h \leq 0.94$ to $0.92 \leq R/h \leq 0.82$ (Fig. 6), the corresponding distributions shift monotonically on the left (lowest f values).

Finally, Fig. 3c confirms that this trend is independent of the chosen R/h ranges, as the overland flow (Savat, 1980) and rough rill (Lucchese et al., 2025) conditions are characterized by the highest f values, while the transition condition (smooth flume by Lucchese et al., 2025) leads to the lowest friction factors.

3.2. Calibration and testing of the theoretical flow resistance equation

The theoretical flow resistance equation (Eq. (19) coupled with Eq. (18) has the advantage of considering the following aspects to be examined when a single resistance law must be applied for all geometrical conditions varying from VWR (overland flows) to NR (rill flows):

1) the variability of flow regime, from the laminar conditions, typical of overland flows, to turbulent conditions, characteristic of rill flows, is represented by Re;
2) the shape of the rectangular cross-section, varying continuously from VWR to NR, is represented by the ratio R/h (see Eq.7);
3) the introduction of F allows for considering all hydraulic conditions from subcritical to supercritical and to include the effects of the depth sediment ratio h/d (Ferro, 2018b);
4) the introduction of slope s allows for distinguishing different hydraulic (flow depth and velocity) and sediment transport (flow transport capacity) conditions (Di Stefano et al., 2021a; Nicosia et al., 2022).

For both calibrating and testing the theoretical flow resistance law (Equations (18) and (19), the complete data set (made of the 702 measurements by Savat (1980) and 196 by Lucchese et al. (2025)) was divided into two sub-data sets, having the same number of experimental runs (449 data) and assuring comparable ranges of the experimental variables (s, Q, h, R, V, R/h) (Table 1). The two sub-data sets were constructed by alternately extracting from the complete data set one run for the calibration set and one for the testing set. The aim of this division criterion was to obtain the same number of experimental runs characterized by the same s, Q, h, R, V, and R/h values in order to prevent the testing dataset from being in extrapolation and to ensure that the model was not influenced by the split criterion. Using the calibration dataset to calibrate Eq. (18), the following relationship was obtained:

$$\Gamma_v = 1.1152\frac{F^{1.2272}}{s^{0.5902}Re^{0.1705}(R/h)^{1.2850}} \qquad (23)$$

which is characterized by a determination coefficient of 0.997 and a $RMSE$ of 0.195.

Fig. 7a shows the comparison between the measured Γ values, obtained by Eq. (16) and the measured values of slope, mean flow velocity V, and water depth h, and those calculated by Eq. (23). Fig. 7b shows the comparison between the measured friction factor values and those calculated by Eq. (19) coupled with Eq. (23). Notwithstanding the differences in terms of the Darcy–Weisbach friction factor pointed out in Fig. 5 and in Fig. 6, the proposed theoretical approach assures a reliable estimate of f (characterized by an $RMSE$ of 0.020), also without considering the variability of the roughness condition. No bias in the estimate of the Darcy–Weisbach friction factor by Eq. (19) coupled with Eq. (23) can be recognized, as P_{BIAS} is equal to 0.0142.

For the testing data set (449 data), Fig. 8a, which shows the comparison between the measured Γ values and those calculated by Eq. (23), confirms the good performance of the proposed equation, which is characterized by an $RMSE$ of 0.191. For the same data set, Fig. 8b shows the comparison between the measured friction factor values and those calculated by Eq. (19) coupled with Eq. (23). Fig. 8b confirms good

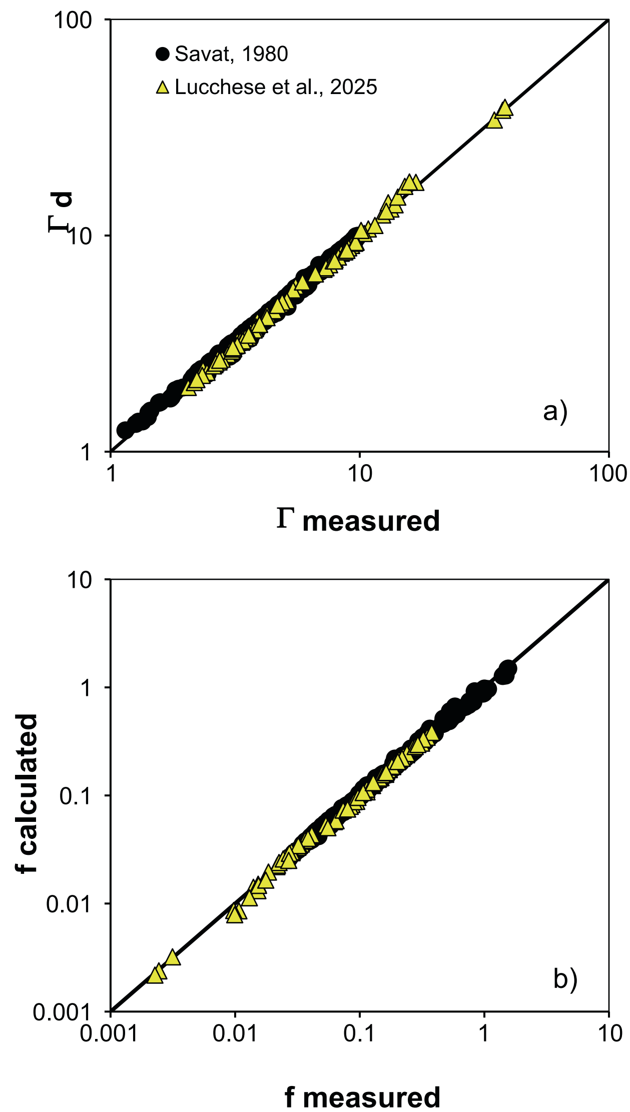

Fig. 7. Comparison, for the calibration dataset, between the measured Γ values obtained by Eq. (16) and those calculated by Eq. (23) (a) and between the measured f values and those calculated by Eqs. (19) and (23) (b).

accuracy also in the f estimate, which is characterized by $RMSE$ of 0.021.

Considering the negligible statistical difference in terms of agreement (Figs. 7 and 8) and $RMSE$ related to the calibration and testing datasets, all the available data (Table 1), which are widely representative of hydraulic conditions varying from VWR to NR, were used to calibrate Eq. (18) and the following relationship was obtained:

$$\Gamma_v = 1.1140\frac{F^{1.2269}}{s^{0.5898}Re^{0.1701}(R/h)^{1.2821}} \qquad (24)$$

which is characterized by a determination coefficient of 0.997 and a $RMSE$ of 0.190.

Fig. 9a shows the comparison between the measured Γ values, obtained by Eq. (16) and the measured values of slope, velocity V and water depth h, and those calculated by Eq. (24). Introducing the coefficients of Eq. (24) into Eq. (20), the following flow resistance equation is obtained:

$$f = 8\left[\frac{(\delta+1)(\delta+2)}{2^{1-\delta}4.9926}\right]^{\frac{2}{1+\delta}}\left(\frac{s^{0.5898}Re^{0.1701}}{F^{1.2269}}\right)^{\frac{2}{1+\delta}}\left[(R/h)^{1.2821}\right]^{\frac{2}{1+\delta}} \qquad (25)$$

Fig. 9b shows the comparison between the measured friction factor

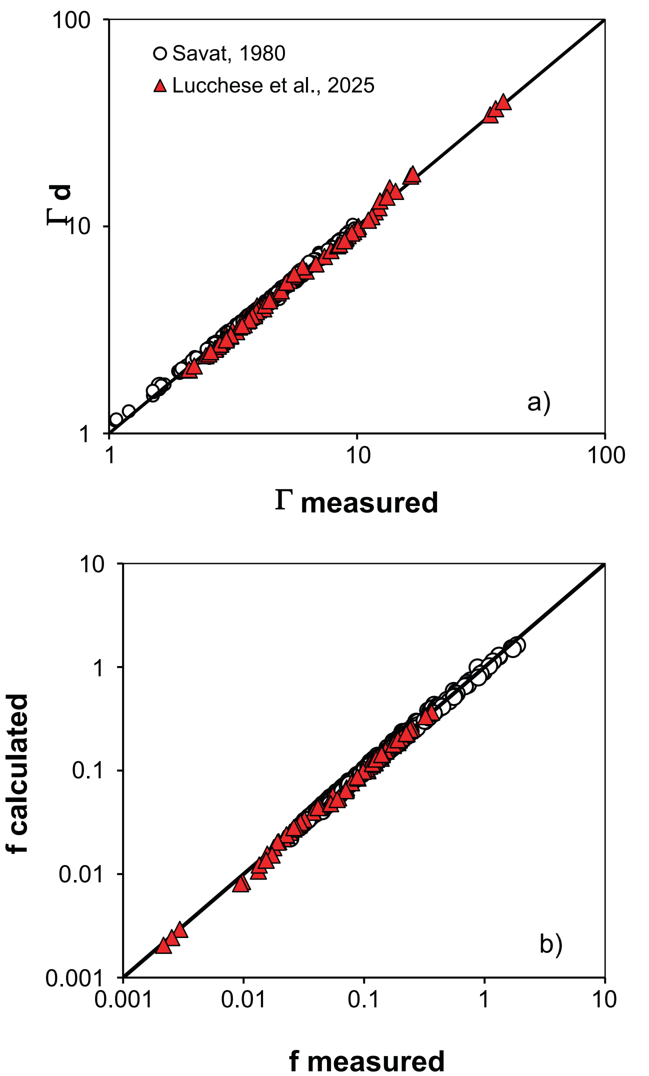

Fig. 8. Comparison, for the testing dataset, between the measured Γ values obtained by Eq. (16) and those calculated by Eq. (23) (a) and between the measured f values and those calculated by Eqs. (19) and (23) (b).

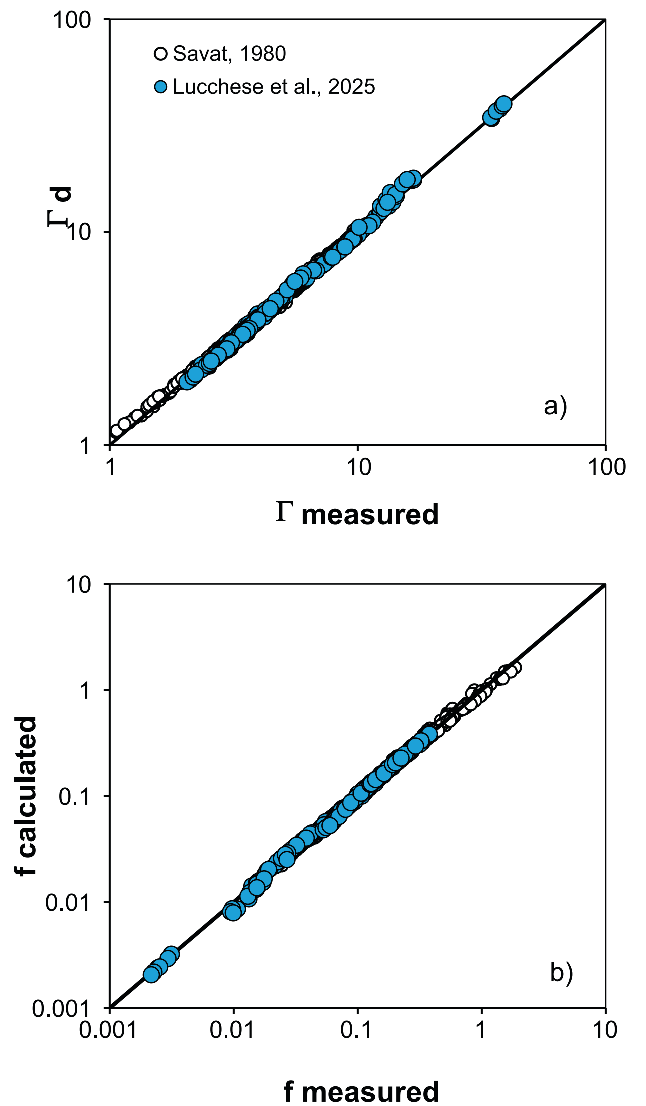

Fig. 9. Comparison, for the whole dataset by Savat (1980) and Lucchese et al. (2025), between the measured Γ values obtained by Eq. (16) and those calculated by Eq. (24) (a) and between the measured f values and those calculated by Eqs. (19) and (24) (b).

values and those calculated by Eq. (25) which is characterized by a *RMSE* = 0.02. Notwithstanding the differences in terms of the Darcy–Weisbach friction factor pointed out in Fig. 5, Fig. 9b confirms that the proposed theoretical approach assures a reliable estimate of f also without considering the variability of roughness condition. The empirical frequency distribution of the errors in estimate E is plotted in Fig. 10. This figure also shows that the errors E are distributed according to a normal law with mean and standard deviation equal to those of the sample empirical errors. Furthermore, the empirical frequency distribution of E is characterized by a sample mean of −0.37, a skewness of −0.24, and a kurtosis of 2.62. For the normal distribution, these values are equal to 0 (mean), 0 (skewness), and 3 (kurtosis).

The analysis of residual $RES = f_m - f_c$ of the Darcy–Weisbach friction factor against the controlling variables (F, s, Re, R/h) was developed, and no systematic bias was recognized. No bias in the estimate of the Darcy–Weisbach friction factor by Eq. (19) coupled with Eq. (24) can be recognized, as P_{BIAS} is equal to 0.0153.

Fig. 11 shows the variability of the experimental δ values, calculated by Eq. (15), and the corresponding R/h values. This figure demonstrates that the hypothesis to assume a constant value of δ can only be applied for rill flows.

For an overland flow condition ($0.92 \le R/h \le 0.99$), assuming $R/h =$ 1, Eq. (25) gives:

$$f = 8\left[\frac{(\delta+1)(\delta+2)}{2^{1-\delta}4.9926}\right]^{\frac{2}{1+\delta}}\left(\frac{s^{0.5898}Re^{0.1701}}{F^{1.2269}}\right)^{\frac{2}{1+\delta}} \tag{26}$$

Considering that for $R/h \le 0.92$, δ varies within a narrow range (0.162–0.222) and has a standard deviation of 0.014, its mean value (0.183) can be introduced into Eq. (26), and, for a rill flow condition, the following equation is deduced:

$$f = 1.0076\left(\frac{R}{h}\right)^{2.1675}\left(\frac{s^{0.9971}Re^{0.2876}}{F^{2.0742}}\right) \tag{27}$$

3.3. Testing the theoretical flow resistance equation by measurements carried out in this investigation

For testing the theoretical flow resistance (Eq. (25), the measurements carried out in this investigation, characterized by values of the experimental variables (s, Q, h, R, V, R/h) falling within the range of the literature data (Table 1), were used.

For this new dataset, Fig. 12a, which shows the comparison between

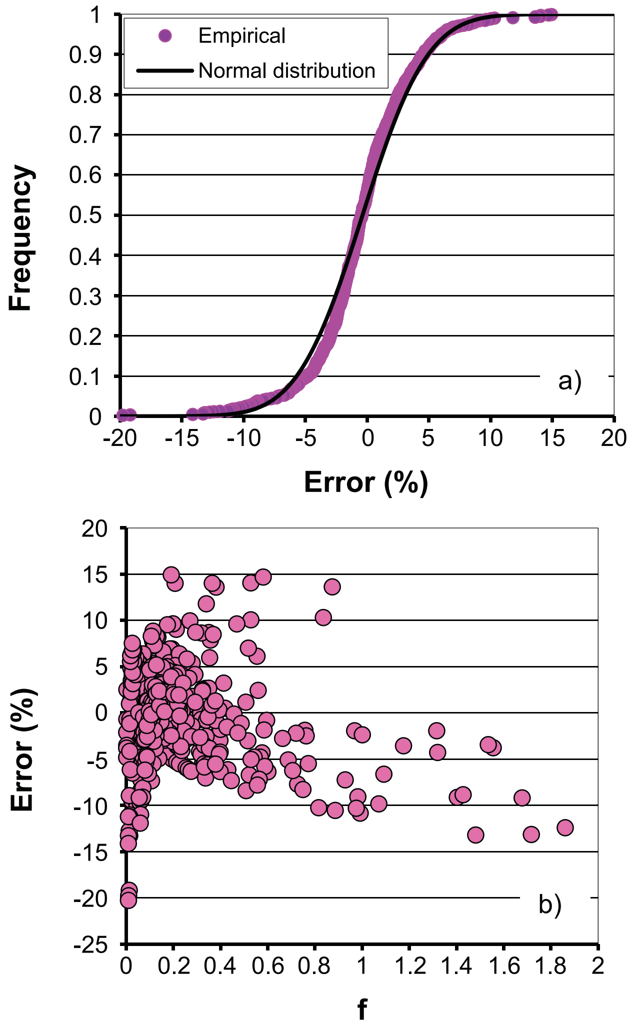

Fig. 10. Empirical frequency distribution of the errors E in the f estimate (a) and relationship between the errors E in the f estimate and the Darcy–Weisbach friction factor (b).

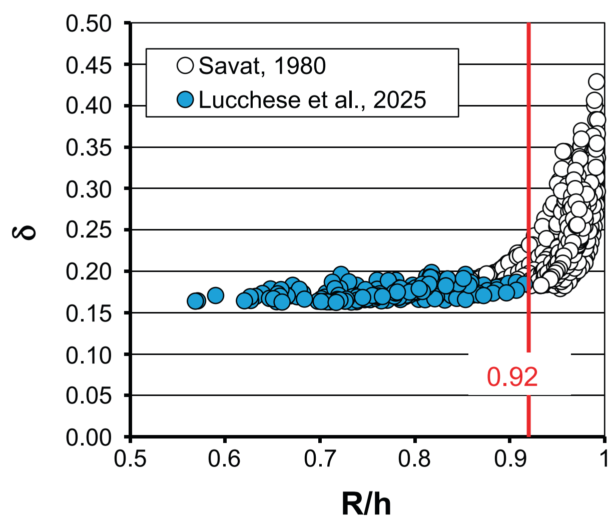

Fig. 11. Variability of the experimental δ values, calculated by Eq. (15), and the corresponding R/h values.

the measured Γ values, obtained by Eq. (16) and the measured values of

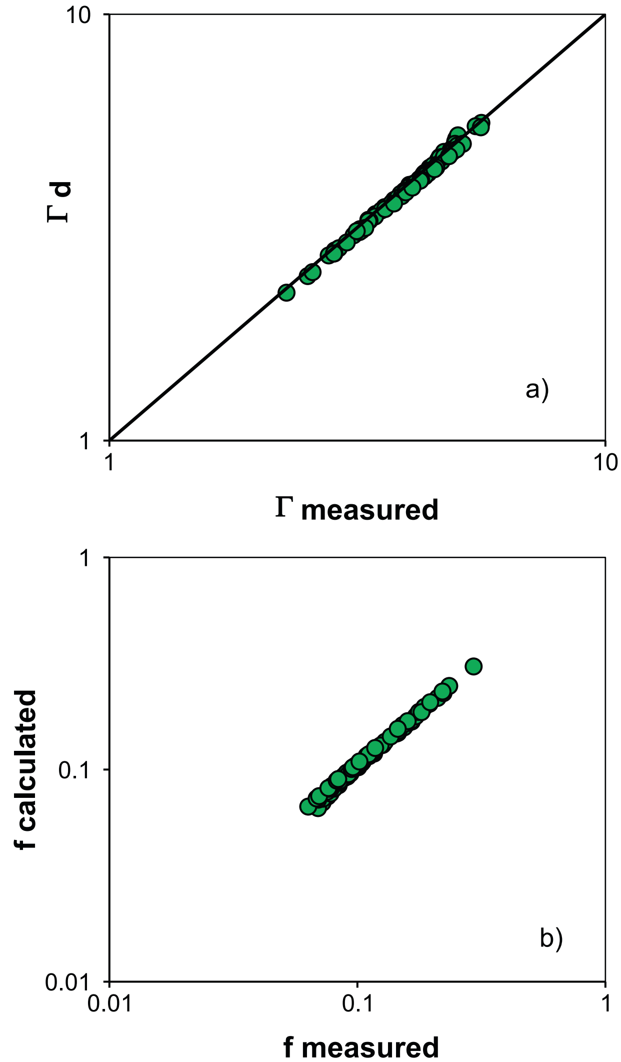

Fig. 12. Comparison, for the measurements performed in this investigation, between the measured Γ values and those calculated by Eq. (24) (a) and between the measured f values and those calculated by Eqs. (19) and (24) (b).

slope, mean flow velocity V, and water depth h, and those calculated by Eq. (24), confirms the good performance of the proposed equation, which is characterized by an *RMSE* of 0.109.

Fig. 12b, which shows the comparison between the measured friction factor values and those calculated by Eq. (25), demonstrates good accuracy in the f estimate, characterized by an *RMSE* of 0.006, also for the testing independent dataset.

4. Discussion

4.1. Evidence from experimental data

Data listed in Table 2 and frequency distributions shown in Fig. 5 pointed out that the investigated ranges of R/h allow for clearly distinguishing between overland and rill flows. The highest f values corresponding to the very wide rectangular cross-sections ($0.99 \leq R/h \leq 0.94$), which are characterized by the highest values of the ratio L/h (9.7 – 270.3), are exclusively due to the bed grain resistance. In fact, only the measurements by Savat (1980) fall in the range $0.99 \leq R/h \leq 0.94$ (Fig. 3b), corresponding to VWR cross-sections, and for these runs the flow resistance contribution due to walls was negligible. Instead, when the narrow rectangular cross-section of rills occurs ($0.80 < R/h \leq 0.57$), the high flow resistance values are due to the prevalent contribution of the channel walls (L/h in the range 2.6 – 7.9). For the database by Savat (1980), the minimum value of R/h (0.82) is greater than the maximum R/h value (0.80) characterizing the NR cross-sections. Thus, in this R/h range (0.80——0.57), only the data by Lucchese et al. (2025) with rough bed conditions, for which the total flow resistance is affected by the contribution due to walls, are included.

For the intermediate geometric conditions ($0.94 < R/h \leq 0.80$), the smallest friction factor values can be justified considering that the resistance contribution of the channel walls is reduced as compared to that of the NR cross-sections.

However, the experimental data evidence that the transition from VWR to NR cross-sections implies a transition in flow resistance conditions related to R/h, and should be represented by the flow resistance equation.

The new analysis of the empirical cumulative frequency distributions corresponding to selected ranges of R/h, identified by samples having the same size ($N = 150$), confirmed the occurrence of the highest f values for overland and rill flow conditions. This analysis also detected a continuity of flow resistance related to the range of R/h, confirming that this variable can effectively represent different flow resistance from VWR to NR cross-sections.

4.2. Calibration and testing of the theoretical flow resistance equation

The analysis developed by subdividing the available data set into two sub-data sets, having the same number of experimental runs (449 data), allowed for calibrating and testing the flow resistance (Eqs. (18) and (19) using two independent sets of measurements. This analysis confirmed that the theoretical approach assures a reliable estimate of the Darcy–Weisbach friction factor and that the f estimates are unbiased.

The agreement between the measured f values and those calculated by Eq. (25) is characterized by good accuracy (Fig. 7), as errors E in estimate (Fig. 8) that, for 96.8% of the cases, are less than or equal to $\pm$ 10% and, for 82.0% of the cases, are less than or equal to $\pm$ 5%. This performance of Eq. (25) is very good notwithstanding the variability of roughness condition (Fig. 5), confirming that F is able to represent the effect of the depth/roughness ratio h/d and, for a given shape of the cross-section (rectangular), the actual influence of soil roughness can be considered negligible (Di Stefano et al., 2024a; Lucchese et al., 2025). According to Di Stefano et al. (2024a) and Lucchese et al. (2025), "…… *for a fixed-bed channel, the effect of the cross-section shape on the Darcy–Weisbach friction factor is much greater than that due to the soil grain size roughness*.". Therefore, the application of Eq. (20) can be carried out using an a value simply representing the category "soil", regardless of the soil texture, as the used measurements are all characterized by rectangular cross-sections. In other words, the change due to the roughness height of different soils does not appreciably affect the estimate of the a coefficient. This finding is confirmed by the circumstance that a single flow resistance equation (Eq. (19) coupled with Eq. (25), with $a = 1.114$) can be applied to all investigated conditions characterized by different roughness (Savat, 1980; Lucchese et al., 2025). In other words, the use of different soils, characterized by different roughness heights, does not significantly affect the estimate of the a coefficient of Eq. (18) and, as a consequence, of the Darcy–Weisbach friction factor.

Considering the theoretical deduction of Eq. (25) and that the errors in estimate f (Fig. 8) are normally distributed (with mean of -0.37 and standard deviation of 4.16), Eq. (25) can be considered a complete model, i.e. Eq. (25) takes into account all the variables required to fully model flow resistance for channels with a rectangular cross-section varying from VWR (overland flows) to NR (rill flows).

4.3. Testing the theoretical flow resistance equation by measurements carried out in this investigation

The measurements carried out in this investigation allowed for a further independent test of the accuracy of Eq. (25) in the estimate of the Darcy–Weisbach friction factor. The *RMSE* of 0.006, corresponding to the estimate of the f value by Eq. (25) for the investigated condition, demonstrates that a high accuracy.

As this investigation also confirmed that the flow resistance results deduced by laboratory measurements with regular cross-sections limit the effects of the soil roughness (Lucchese et al., 2025), future research challenges could be using other experimental channels with different widths and widening the range of investigated slopes s (higher than 15%) and Re for the rill flow condition (Fig. 4).

5. Conclusions

The study of interrill (with overland flows) and channelized (rill and gully) erosion is relevant for modeling soil erosion and transport processes. In this investigation, flume measurements performed by Savat (1980) and Lucchese et al. (2025) in smooth and rough channels, which are characterized by a fixed bed and a grain resistance condition, were firstly used to demonstrate the experimental evidence that a continuity in flow resistance from overland (R quasi equal to h) to rill flows ($R/h < 1$) can be stated. This analysis demonstrated that the highest f values correspond to the very wide rectangular cross-sections ($0.99 \leq R/h \leq 0.94$), typical of overland flows, and to the narrow rectangular sections ($0.80 < R/h \leq 0.57$) corresponding to rill condition, while for the intermediate geometric conditions ($0.94 < R/h \leq 0.80$), the lowest friction factor values were measured. This detected transition from VWR to NR cross-sections implies a transition in flow resistance conditions, and its relationship with R/h was represented by the flow resistance equation. In particular, the theoretical flow resistance law (Eq.20) was deduced considering rectangular cross-sections characterized by different R/h values and calibrated by the available datasets. The agreement between the measured f values and those calculated by Eq. (22) was characterized by good accuracy. The errors E in estimate, which were normally distributed, were less than or equal to $\pm$ 10% for 96.8% of the cases and less than or equal to $\pm$ 5% for 82.0% of the cases. The proposed flow resistance equation is applicable for channels with a rectangular cross-section varying from VWR (overland flows) to NR (rill flows).

Future research could be developed by experimental channels with different channel widths and widening the range of investigated slope s (higher than 15%) and Re for the rill flow condition.

CRediT authorship contribution statement

Vincenzo Palmeri: Writing – review & editing, Writing – original draft, Visualization, Validation, Methodology, Investigation, Formal analysis, Data curation, Conceptualization. **Alessio Nicosia:** Writing – review & editing, Writing – original draft, Visualization, Validation, Methodology, Investigation, Formal analysis, Data curation, Conceptualization. **Costanza Di Stefano:** Writing – review & editing, Writing – original draft, Visualization, Validation, Methodology, Investigation, Formal analysis, Data curation, Conceptualization. **Vito Ferro:** Writing – review & editing, Writing – original draft, Visualization, Validation, Supervision, Methodology, Investigation, Formal analysis, Data curation, Conceptualization.

Declaration of competing interest

The authors declare that they have no known competing financial interests or personal relationships that could have appeared to influence the work reported in this paper.

Acknowledgments

All the authors contributed to outlining the investigation, analyzing the data, discussing the results, and writing the manuscript. This research did not receive any specific grant from funding agencies in the

public, commercial, or not-for-profit sectors.

Data availability

The data are published in the papers by Savat (1980) and Lucchese et al. (2025)

References

Abrahams, A.D., Parsons, A.J., Wainwright, J., 1994. Resistance to overland flow on semiarid grassland and shrubland hillslopes, Walnut Gulch, southern Arizona. J. Hydrol. 156, 431–446.

Bagarello, V., Ferro, V., Flanagan, D., 2018. Predicting plot soil loss by empirical and process-oriented approaches. a review. Journal of. Agri. Eng. Vol. XLIX:710.

Barenblatt, G.I., Monin, A.S., 1979. Similarity laws for turbulent stratified flows. Arch. Ration. Mech. Anal. 70, 307–317.

Barenblatt, G.I., 1987. Dimensional analysis. Gordon and Breach, Science Publishers, Amsterdam, Netherlands.

Barenblatt, G.I., 1991. On the scaling laws (incomplete self-similarity with respect to Reynolds numbers) for the developed turbulent flows in tubes. C. r. Acad. Sci. Ser. II 13, 307–312.

Barenblatt, G.I., 1993. Scaling laws for fully developed turbulent shear flows. I: basic hypothesis and analysis. J. Fluid Mech. 248, 513–520.

Barenblatt, G.I., Prostokishin, V.M., 1993. Scaling laws for fully developed turbulent shear flows, part 2. Processing of experimental data. J. Fluid Mech. 248, 521–529.

Borrelli, P., Robinson, D.A., Fleischer, L.R., Lugato, E., Ballabio, C., Alewell, C., Meusburger, K., Modugno, S., Schütt, B., Ferro, V., Bagarello, V., Van Oost, K., Montanarella, L., Panagos, P., 2017. An assessment of the global impact of 21st century land use change on soil erosion. Nat. Commun. 8, 2013. https://doi.org/10.1038/s41467-017-02142-7.

Capra, A., Di Stefano, C., Ferro, V., Scicolone, B., 2009. Similarity between morphological characteristics of rills and ephemeral gullies in Sicily, Italy. Hydrol. Process. 23, 3334–3341.

Carollo, F.G., Di Stefano, C., Ferro, V., Pampalone, V., 2015. Measuring rill erosion at plot scale by a drone-based technology. Hydrol. Process. 29, 3802–3811.

Carollo, F.G., Di Stefano, C., Nicosia, A., Palmeri, V., Pampalone, V., Ferro, V., 2021. Flow resistance in mobile bed rills shaped in soils with different texture. Eur. J. Soil Sci. 72, 2062–2075.

Casalì, J., Loizu, J., Campo, M.A., De Santisteban, L.M., Àlvarez – Mozos, J., 2006. Accuracy of methods for field assessment of rill and ephemeral gully erosion. Catena 67, 128–138.

Castaing, B., Gagne, Y., Hopfinger, E.J., 1990. Velocity probability density functions of high Reynolds number turbulence. Phys. D 46, 177–200.

Dan, C., Liu, G., Zhao, Y., Shu, C., Shen, E., Liu, C., Tan, Q., Zhang, Q., Guo, Z., Zhang, Y., 2023. The effects of typical grass cover combined with biocrusts on slope hydrology and soil erosion during rainstorms on the Loess Plateau of China: an experimental study. Hydrol. Process. 37 (1), e14794.

Dan, C., Liu, G., Zhang, Q., Zhao, Y., Shen, E., Liu, C., Liu, Y., Shu, C., Xia, X., Liu, D., Guo, Z., 2024. The coupling effects of grass and shrub with biological crust on the overland flow hydrodynamic characteristics. Catena 245, 108281.

De Roo, A.P.J., Wesseling, C.G., Cremers, N.H.D.T., Offermans, R.J.E., Ritsema, C.J., Van Oostindie, K., 1994. LISEM: a new physically-based hydrological and soil erosion model in a GIS-environment, theory and implementation. In: Variability in Stream Erosion and Sediment Transport (Proceedings of the Canberra Symposium), pp. 439–448. IAHS Publ. no. 224.

Di Stefano, C., Ferro, V., 2011. Measurements of rill and gully erosion in Sicily. Hydrol. Process. 25, 2221–2227.

Di Stefano, C., Ferro, V., Palmeri, V., Pampalone, V., 2018. Testing slope effect on flow resistance equation for mobile bed rills. Hydrol. Process. 32, 664–671.

Di Stefano, C., Nicosia, A., Palmeri, V., Pampalone, V., Ferro, V., 2019. Comparing flow resistance law for fixed and mobile bed rills. Hydrol. Process. 2019 (33), 3330–3348.

Di Stefano, C., Nicosia, A., Palmeri, V., Pampalone, V., Ferro, V., 2021a. Estimating flow resistance in steep slope rills. Hydrol. Process. 35, e14296.

Di Stefano, C., Nicosia, A., Palmeri, V., Pampalone, V., Ferro, V., 2021b. Flume experiments for assessing the dye-tracing technique in rill flows. Flow Meas. Instrum. 77 (2), 101870.

Di Stefano, C., Nicosia, A., Palmeri, V., Pampalone, V., Ferro, V., 2022a. Rill flow velocity and resistance law: a review. Earth Science Review 231, 104092. https://doi.org/10.1016/j.earscirev.2022.104092.

Di Stefano, C., Nicosia, A., Palmeri, V., Pampalone, V., Ferro, V., 2022b. Rill flow resistance law under sediment transport. J. Soil. Sediment. 22, 334–347. https://doi.org/10.1007/s11368-021-03083-x.

Di Stefano, C., Nicosia, A., Pampalone, V., Palmeri, V., Ferro, V., 2024a. Evaluating the effects of soil grain roughness and rill cross-section shape on flow resistance. Hydrol. Process. 38, e15119. https://doi.org/10.1002/hyp.15119.

Di Stefano, C., Guida, G., Nicosia, A., Palmeri, V., Pampalone, V., Ferro, V., 2024b. Effects of surface inoculation of biological soil crusts on laminar overland flow resistance. Hydrol. Process. 38 (6), e15198.

Emmett, W.W., 1970. The hydraulics of overland flow on hillslopes: Dynamic and descriptive studies of hillslopes. Geol. Surv. Prof. Pap. A1–A67.

Fang, C., Pan, X., Zhang, B., Zhang, K., Lv, X., 2021. An experimental study on the evolution law of roll wave parameters in overland flow. Hydrol. Process. 35, e14408. https://doi.org/10.1002/hyp.14408.

Ferro, V., 1997. Applying hypothesis of self-similarity for flow-resistance law of small-diameter plastic pipes. J. Irrig. Drain. Eng. https://doi.org/10.1061/(ASCE)0733-9437(1997)123:3(175), 175-179.

Ferro, V., 2003. ADV measurements of velocity distributions in a gravel-bed flume. Earth Surf. Proc. Land. 28 (7), 707–722.

Ferro, V., 1999. Friction factor for gravel-bed channel with high boulder concentration. J. Hydraul. Eng. 125, 771–778. https://doi.org/10.1061/(ASCE)0733-9429(1999)125:7(771).

Ferro, V., 2010. Deducing the USLE mathematical structure by dimensional analysis and self-similarity theory. Biosyst. Eng. 106 (2), 216–220.

Ferro, V., 2017. New flow-resistance law for steep mountain streams based on velocity profile. J. Irrig. Drain. Eng, ASCE 143 (04017024), 1–6. https://doi.org/10.1061/(ASCE)IR.1943 4774.0001208.

Ferro, V., 2018a. Flow resistance law under equilibrium bed-load transport conditions. Flow Meas. Instrum. 64, 1–8. https://doi.org/10.1016/j.flowmeasinst.2018.10.008.

Ferro, V., 2018b. Assessing flow resistance in gravel bed channels by dimensional analysis and self-similarity. Catena 169, 119–127. https://doi.org/10.1016/j.catena.2018.05.034.

Ferro, V., Nicosia, A., 2020. Comment on "Rill erosion processes on steep colluvial deposit slope under heavy rainfall in flume experiments with artificial rain by F. Jiang et al. Catena 185, 103793.

Ferro, V., Pecoraro, R., 2000. Incomplete self-similarity and flow velocity in gravel bed channels. Water Resour. Res. 36, 2761–2770.

Ferro, V., Porto, P., 2018. Applying hypothesis of self-similarity for flow resistance law in Calabrian gravel-bed rivers. J. Hydraul. Eng. ASCE 140 (04017061), 1–11. https://doi.org/10.1061/(ASCE)HY.1943-7900.0001385.

Flanagan, D.C., Gilley, J.E., Franti, T.G., 2007. Water erosion Prediction Project (WEPP): development history, model capabilities, and future enhancements. Trans. of the ASABE 50 (5), 1603–1612.

Flanagan, D.C., Nearing, M.A., 1995. USDA Water Erosion Prediction Project hillslope profile and watershed model documentation. NSERL Report No. 10. West Lafayette, Ind.: USDA-ARS National Soil Erosion Research Laboratory.

Foster, G.R., Flanagan, D.C., Nearing, M.A., Lane, L.J., Risse, L.M., Finkner, S.C., 1995. Chapter 11. Hillslope erosion component. In: Flanagan, D.C., Nearing, M.A. (Eds.), USDA Water Erosion Prediction Project Hillslope Profile and Watershed Model Documentation. NSERL Report No. 10. USDA-ARS National Soil Erosion Research Laboratory, West Lafayette, Ind, 12 pp.

Foster, G.R., Huggins, L.F., Meyer, L.D., 1984. A laboratory study of rill hydraulics: I. Velocity Relationships. Trans. ASAE 27, 790–796.

Gilley, J.E., Kottwitz, E.R., Simanton, J.R., 1990. Hydraulics characteristics of rills. Trans. ASAE 33 (6), 1900–1906.

Govers, G., 1992. Relationship between discharge, velocity and flow area for rills eroding loose, non-layered materials. Earth Surf. Proc. Land. 17, 515–528.

Govers, G., Gimenez, R., Van Oost, K., 2007. Rill erosion: Exploring the relationship between experiments, modelling and field observations. Earth Sci. Rev. 84, 87–102.

Govers, G., Takken, I., Helming, K., 2000. Soil roughness and overland flow. Agronomie 20 (2), 131–146. https://doi.org/10.1051/agro:2000114.

Gupta, H.V., Sorooshian, S., Yapo, P.O., 1999. Status of automatic calibration for hydrologic models: Comparison with multilevel expert calibration. J. Hydrol. Eng. 4 (2), 135–143. https://doi.org/10.1061/(ASCE)1084-0699(1999)4:2(135).

Hessel, R., Jetten, V., Guanghui, Z., 2003. Estimating Manning's n for steep slopes. Catena 54 (1–2), 77–91.

Horton, R.E., 1945. Erosional development of streams and their drainage basins; hydrophysical approach to quantitative morphology. Geol. Soc. Am. Bull. 56 (3), 275–370.

Laflen, J.M., Lane, L.J., Foster, G.R., 1991. WEPP: a new generation of erosion prediction technology. J. Soil Water Conserv. 46 (1), 34–38.

Liu, C., Fu, S., Li, Z., Zhang, Z., Zeng, J., 2023. Effects of sediment characteristics on the sediment transport capacity of overland flow. International Soil and Water Conservation Research 11 (1), 75–85.

Lucchese, A., Nicosia, A., Palmeri, V., Pampalone, V., Ferro, V., 2025. Influence of soil grain roughness and roughness type on flow resistance in rectangular rill channels. Hydrol. Process. 39, e70238. https://doi.org/10.1002/hyp.70238.

Morgan, R.P.C., Quinton, J.N., Smith, R.E., Govers, G., Poesen, J.W.A., Auerswald, K., Chisci, G., Torri, D., Styczen, M.E., 1998. The European Soil erosion Model (EUROSEM): a dynamic approach for predicting sediment transport from fields and small catchments. Earth Surf. Proc. Land. 23 (6), 527–544.

Mutchler, C.K., Young, R.A., 1975. Soil detachment by raindrops. In: Present and Prospective Technology for Predicting Sediment Yield and Sources, ARS-S-40. USDA Science and Education Administration, Washington, DC, pp. 113–117.

Nearing, M.A., Foster, G.R., Lane, L.J., Finkner, S.C., 1989. A process-based soil erosion model for USDA-Water erosion Prediction Project technology. Trans. of the ASAE 32 (5), 1587–1593.

Nearing, M.A., Norton, L.D., Bulgakov, D.A., Larionov, G.A., West, L.T., Dontsova, K.M., 1997. Hydraulics and erosion in eroding rills. Water Resour. Res. 33, 865–876.

Nicosia, A., Carollo, F.G., Di Stefano, C., Palmeri, V., Pampalone, V., Ferro, V., 2024a. Overland flow resistance: a review. Earth Sci. Rev. 258, 104949. https://doi.org/10.1016/j.earscirev.2024.104949.

Nicosia, A., Di Stefano, C., Ferro, V., 2025a. Rainfall effects on overland flow resistance. J. Hydrol. 662, 133838. https://doi.org/10.1016/j.jhydrol.2025.133838.

Nicosia, A., Di Stefano, C., Ferro, V., 2025b. Study on overland flow resistance under simulated rainfall. Hydrol. Process. 39, e70236. https://doi.org/10.1002/hyp.70236.

Nicosia, A., Di Stefano, C., Palmeri, V., Pampalone, V., Ferro, V., 2020a. Flow resistance of overland flow on a smooth bed under simulated rainfall. Catena 187, 104351. https://doi.org/10.1016/j.catena.2019.104351.

Nicosia, A., Di Stefano, C., Palmeri, V., Pampalone, V., Ferro, V., 2021a. Roughness effect on the correction factor of surface velocity for rill flows. Hydrol. Process. 35, e14407. https://doi.org/10.1002/hyp.14407.

Nicosia, A., Di Stefano, C., Pampalone, V., Palmeri, V., Ferro, V., Nearing, M.A., 2019. Testing a new rill flow resistance approach using the water erosion prediction project experimental database. Hydrol. Process. 33, 616–626.

Nicosia, A., Di Stefano, C., Pampalone, V., Palmeri, V., Ferro, V., Nearing, M.A., 2020b. Testing a theoretical resistance law for overland flow on a stony hillslope. Hydrol. Process. 34 (9), 2048–2056.

Nicosia, A., Di Stefano, C., Palmeri, V., Serio, M.A., Ferro, V., 2024b. Assessing a transitional and turbulent overland flow resistance law for surfaces with different roughness. J. Hydrol. 641, 131858. https://doi.org/10.1016/j.jhydrol.2024.131858.

Nicosia, A., Di Stefano, C., Pampalone, V., Palmeri, V., Ferro, V., 2021b. Assessing an overland flow resistance approach under equilibrium sediment transport conditions. Catena 207, 105578.

Nicosia, A., Palmeri, V., Pampalone, V., Di Stefano, C., Ferro, V., 2022. Slope threshold in rill flow resistance. Catena 208, 105789.

Nouwakpo, S.K., Williams, C.J., Al-Hamdam, O.Z., Weltz, M.A., Pierson, F., Nearing, M., 2016. A review of concentrated flow erosion processes on rangelands: fundamental understanding and knowledge gaps. Int. Soil Water Conserv. Res. 4, 75–86.

Palmeri, V., Pampalone, V., Di Stefano, C., Nicosia, A., Ferro, V., 2018. Experiments for testing soil texture effects on flow resistance in mobile bed rills. Catena 171, 176–184.

Pampalone, V., Nicosia, A., Palmeri, V., Serio, M.A., Ferro, V., 2023. Rill and interrill soil loss estimations using the USLE-MB equation at the Sparacia Experimental Site (South Italy). Water 15 (13), 2396.

Peng, W., Zhang, Z., Zhang, K., 2015. Hydrodynamic characteristics of rill flow on steep slopes. Hydrol. Process. 29, 3677–3686.

Powell, D.M., 2014. Flow resistance in gravel-bed rivers: progress in research. Earth Sci. Rev. 136, 301–338.

Savat, J., 1980. Resistance to flow in rough supercritical sheet flow. Earth Surf. Processes 5 (2), 103–122.

Shen, E., Liu, G., Jia, Y., Dan, C., Abd Elbasit, M.A., Liu, C., Gu, J., Shi, H., 2021. Effects of raindrop impact on the resistance characteristics of sheet flow. J. Hydrol. 592, 125767.

Shen, E., Liu, G., Dan, C., Chen, X., Ye, S., Li, R., Li, H., Zhang, Q., Zhang, Y., Guo, Z., 2023a. Estimating Manning's coefficient n for sheet flow during rainstorms. Catena 226, 107093.

Shen, E., Liu, G., Xia, X., Dan, C., Zheng, F., Zhang, Q., Zhang, Y., Guo, Z., 2023b. Resistance to sheet flow induced by raindrop impact on rough surfaces. Catena 231, 107272.

Smith, M.W., Cox, N.J., Bracken, L.J., 2007. Applying flow resistance equations to overland flows. Prog. Phys. Geogr. 31 (4), 363–387.

Toy, T.J., Foster, G.R., Renard, K.G., 2002. Soil erosion: processes, prediction, measurement, and control. John Wiley & Sons Inc, New York.

Wang, J., Zhang, K., Li, P., Meng, Y., Zhao, L., 2021. Hydrodynamic characteristics and evolution law of roll waves in overland flow. Catena 198, 105068. https://doi.org/10.1016/j.catena.2020.105068.

Wang, X.K., Yan, X.F., Zhou, S.F., Huang, E., Liu, X.N., 2014. Longitudinal variations of hydraulic characteristics of overland flow with different roughness. J. Hydrodyn. 26 (1), 66–74. https://doi.org/10.1016/S1001-6058(14)60008-1.

Zanuttigh, B., Lamberti, A., 2002. Roll waves simulation using shallow water equations and Weighted Average Flux method. J. Hydraul. Res. 40 (5), 610–622. https://doi.org/10.1080/00221680209499905.